U.S. DEPARTMENT OF THE INTERIOR
U.S. GEOLOGICAL SURVEY

Prepared in cooperation with the
U.S. DEPARTMENT OF ENERGY, under
Interagency Agreement DE–AI08–92NV10874

MISCELLANEOUS INVESTIGATIONS SERIES
MAP I-2590 (Sheet 1 of 2)

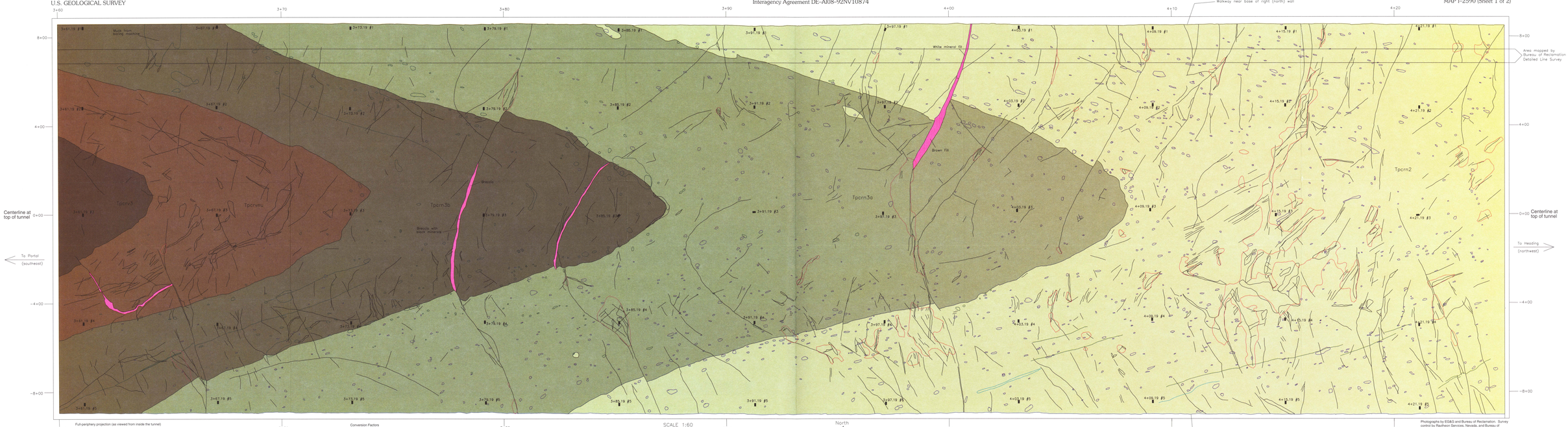

Full-periphery projection (as viewed from inside the tunnel)
Tunnel excavated by Tunnel Boring Machine (TBM)
Mapped by photogrammetric methods from close-range photographs taken in March and April 1995
Units shown are meters. Units on the horizontal axis represent stationing coordinates in an engineering format typically used for tunnels. For example, 3+40 refers to 360 meters from the portal of the tunnel. Units on the vertical axis refer to the distance down the wall away from the centerline, which is at 0+00. Positive and negative designations distinguish the north and south tunnel walls, respectively.

Conversion Factors		
Multiply	By	To obtain
centimeter (cm)	0.3937	inch (in.)
kilometer (km)	0.6214	mile (mi)
meter (m)	3.281	foot (ft)
millimeter (mm)	0.03937	inch (in.)
square meter (m^2)	10.76	square foot (ft^2)

SCALE 1:60
0 1 2 3 4 5 6 7 8 9 10 METERS
0 5 10 15 20 25 30 FEET

North
299°

Photographs by EG&G and Bureau of Reclamation. Survey control by Raytheon Services, Nevada, and Bureau of Reclamation. Map produced at the U.S. Geological Survey using ARC/INFO and Intergraph MGE software between July and September 1996. (Reviewed by Sherilyn Williams-Stroud and Warren Day.)

INTRODUCTION

The Exploratory Studies Facility (ESF) is a 7.9-km-long tunnel being excavated by tunnel-boring machine at Yucca Mountain, Nevada (fig. 1), the site selected by the U.S. Congress for characterization as a potential repository for storage of high-level nuclear waste (U.S. Department of Energy, 1988). The ESF provides underground access and exposure to critical lithostratigraphic horizons for the purpose of geologic mapping and engineering and hydrologic testing. The potential repository is designed to be located in the Topopah Spring Tuff, the oldest formation of the Paintbrush Group of Miocene age (Sawyer and others, 1994). Additional units in the Paintbrush Group exposed in the ESF include the Pah Canyon Tuff, Yucca Mountain Tuff, and Tiva Canyon Tuff in ascending stratigraphic order.

Current requirements place the repository at least 200 m below the surface of Yucca Mountain in the unsaturated zone. Detailed mapping of the fracture network at Yucca Mountain is considered an essential element in the characterization of the potential repository because the network provides potential hydraulic and pneumatic pathways to and from the repository. Flow of fluid and gas through the fracture network depends, in part, on how well fractures are connected. Additional information on orientation, spacing (intensity), aperture/trace-length relations, lateral and vertical variability, and other physical characteristics of fractures in the network provides input for fluid flow and tectonic models of the site. Unfortunately, detailed fracture data such as those described above are generally difficult to acquire at Yucca Mountain because of a lack of exposed and (or) accessible outcrop on the surface or because construction and safety constraints in the ESF limit the amount of data that can be collected. The photogrammetric method used to produce this map eliminates some of these difficulties by reducing the amount of time required for data collection onsite, by providing the capability to map and analyze data from inaccessible exposures, and by allowing for the collection of detailed fracture data that can be impractical to collect using manual field mapping techniques (for example, collection of characteristics of fractures less than 1 m in length, the typical mapping cutoff used by many conventional techniques). Additionally, the photogrammetric method provides digital three-dimensional spatial and attribute data for Geographic Information System (GIS) analysis.

The geologic- and fracture-mapping program in the ESF consists of three components—conventional full-periphery mapping at a scale of 1:125, detailed line-survey mapping within a 60-cm-wide swath along a single rib of the tunnel, and close-range (camera-to-object distance less than 300 m) photogrammetric geologic mapping at a scale of 1:60. Conventional full-periphery mapping and detailed line surveys are being done throughout the ESF, whereas close-range photogrammetric mapping is being done only at sites for which detailed geologic mapping is needed to address specific problems.

This map report presents data from photogrammetric mapping at one site located on the north ramp of the ESF between stations 3+60 and 4+25 meters (fig. 1). The site was selected for mapping because (1) it is one of the first non-obstructed (free of concrete and steel support) sections of bored tunnel that is accessible for use by the photogrammetric technique, and (2) the site is in the crystal-rich member of the Tiva Canyon Tuff, a stratigraphic position for which little detailed fracture data were previously available.

MAPPING PROCEDURES

The photogrammetric mapping method consisted of placing and surveying photogrammetric targets on the walls of the tunnel, photographing the walls using a medium (60-mm frame-size) format camera to obtain blocks of overlapping stereophotographs, and orienting the photographs to the targets by using a Kern DSR15[1] analytical stereoplotter. Once the photographs were properly oriented in the analytical plotter, three-dimensional linework and attribute information was collected. Attitudes[2] were calculated by using a least-squares adjustment and the generic equation of a plane to find the best fit of a planar surface to points measured on individual geologic features (Daeholm, 1979; Daeholm and Coe, 1989; Daeholm and Pillmore, 1989). ArcCAD GIS and DIPS stereographic software was used for data analysis. Additional details regarding the photogrammetric method and its application to structural analysis have been described previously (Coe, 1995) and will not be further discussed in this map report.

The mapping approach used was the inventory method (Davis, 1984), which entails mapping all geologic features observed at the site. In general, features with a single dimension (for example, length or width) larger than approximately 10 cm were readily visible and identifiable for mapping purposes. All visible contacts, lithic and pumice fragments, mineralized and non-mineralized cavities, vapor-phase partings, and bedding traces were mapped. Additionally, all fractures having trace lengths greater than about 15 cm were mapped. For each fracture mapped, the following information was recorded from stereo observations: Fracture label, rib on which the fracture was observed, strike, dip, dip direction, strike error, dip error, planar-surface error, presence and type of mineral fill, maximum wall separation, planarity, and termination. Mineral fill was recorded as the occurrence of white, brown, or black minerals because accurate identification of minerals was not possible from the photographs alone. Additionally, any observable slickenside striations, offset relations, alteration rinds, gas tubules, or mode of formation (shear or extension) information were recorded. Trace length was not recorded as an attribute initially but was calculated later from digitized fracture points in ArcCAD. The errors on strike, dip, and the calculated plane were generated by the least-squares adjustment. These errors are representative of real errors in measurement and, more predominantly, of the natural deviation of the actual fracture surface from a flat planar surface.

The map is shown in a full-periphery projection (fig. 2), as viewed from the inside of the tunnel. The full-periphery projection uses the design dimensions of the tunnel (a 7.62-m-diameter cylinder) and projects the mapped data onto the walls of this theoretical tunnel by using the radius from the theoretical centerline (Daeholm, 1989; Coe, 1995). The projection can be viewed as if observed from outside or inside the tunnel (fig. 3). The inside view of the projection is the same as the view provided by the stereophotographs and is therefore most useful when comparing the mapped fractures to the photographs. A disadvantage of using the inside view for ESF data is that the view results in a map that has east to the left and west to the right, a condition opposite that of most plan view maps. The outside view is useful because it provides a similar perspective to that produced by a plan view map but also displays fractures mapped on the ribs of the tunnel. The outside view is used for conventional full-periphery mapping in the ESF. It should be noted that although the term "full-periphery projection" is used throughout the report, the projection does not include the floor (sill) of the tunnel and is therefore truly a three-quarters-periphery projection.

Although spatial data in this report are shown in the inside view, any of the projections shown in figure 3 are possible because the data are three dimensional. Also, by linking the spatial data (linework) in ArcCAD with the attribute data (see enclosed tabular listing of attribute data), many different types of thematic maps can be produced from the data set. For example, a map could easily be produced of all fractures with strike values between 60 and 80 and trace lengths greater than 2 m.

RESULTS

The site was mapped using 170, 1:90-scale photographs. Orientation of these photographs and geologic mapping took about 100 hours on the analytical plotter. More than one thousand (1,171) fractures were mapped from the photographs. Analysis of these fractures and their attributes (see enclosed tabular listing) provides the following observations.

About 90 percent of fractures at the site have dips between 50 and 90 and strikes that range from 120 to 260 and 310 to 70 (fig. 4). Fractures with a component of dip to the west are more abundant than those with a component of dip to the east. There is considerable variability in the fracture distributions when subdivided on a unit-by-unit basis (figs. 5–9). The Tiva Canyon Tuff crystal-rich member vitric zone (Tpcrvnu), for example, contains roughly equal proportions of shallow and steeply dipping fractures (fig. 6). Additionally, the average strike of the major concentration(s) of fractures appears to change downsection into the lower part of the crystal-rich member, from about 193 in unit Tpcrn3b, to 193 and 171 in unit Tpcrn3a, to 160 in unit Tpcrn2 (figs. 7–9).

Fractures with mineral fill or coatings make up about 11 percent of all fractures mapped (fig. 10) and have attitudes that are distributed roughly the same as the overall fracture distribution (fig. 4). Shear displacement was documented along about 3 percent of mapped fractures. Seventy-two percent of these shear fractures have strikes to the north-northeast, between 180 and 220 or between 340 and 360 (fig. 11). Generally, fractures with shear displacement also contain mineral fill or coatings. The maximum amount of apparent dip-slip displacement along a shear fracture in the map area was 1.2 m. The average strike and dip of contacts in the map area was 8 and 16, respectively (fig. 12).

Seventy percent of the fractures mapped have trace lengths less than 1 m, and 89 percent have trace lengths less than 2 m (fig. 13). The distribution of trace lengths is consistent with a power-law distribution model down to the 15-cm mapping cutoff. Median trace-length values show a positive correlation with maximum wall separation (fig. 14). The longest fractures therefore tend to have the widest wall separations, and the shortest fractures tend to have the narrowest wall separations.

The average fracture intensity ranges from 0.56 fracture/m^2 in the nonwelded to partially welded subzone of the crystal-rich member (Tpcrv3) to 1.85 fracture/m^2 in the vitric to subvitric subzone (Tpcrvnu; fig. 15). The percentage of abutting fracture terminations ranges from 11 to 26 percent (fig. 16). Surprisingly, the unit that contains the highest intensity of fracturing (Tpcrvnu, fig. 15) is not the same unit that has the highest percentage of abutting fracture terminations (Tpcrn3b, fig. 16), although this observation may be due to the fact that fracture crossings are not included in the analysis.

Shallow-dipping fractures are missing from within the detailed line survey swath (fig. 17). Also, the distribution of trace lengths from the detailed line survey swath (fig. 18) contains a proportionally lower number (49 percent) of short (less than 1 m) fractures than does the distribution of trace lengths from the entire map area (70 percent, fig. 13). These observations indicate that the detailed line survey mapping method may be somewhat biased against short and shallow-dipping fractures.

REFERENCES CITED

Buesch, D.C., Spengler, R.W., Moyer, T.C., and Geslin, J.K., 1996, Revised stratigraphic nomenclature and macroscopic identification of lithostratigraphic units of the Paintbrush Group exposed at Yucca Mountain, Nevada: U.S. Geological Survey Open-File Report 94–469, 52 p.

Coe, J.A., 1995, Close-range photogrammetric, geologic mapping and structural analysis, Henderson Mine, Empire, Colo.: Golden, Colorado School of Mines, Master's thesis T–4491 [unpublished], 192 p.

Davis, G.H., 1984, Structural geology of rocks and regions: New York, Wiley & Sons, 492 p.

Daeholm, K.S., 1979, Geologic and topographic mapping from aerial photographs, *in* Geologic and topographic mapping from aerial photographs: Lyngby, The Institute of Surveying and Photogrammetry, The Technical University of Denmark, p. 9–146.

Daeholm, K.S., 1989, GEOPROGRAM—A program for geologic photogrammetry on the Kern DSR analytical plotter, users manual: U.S. Geological Survey Open-File Report 89–481, 47 p.

Daeholm, K.S., and Coe, J.A., 1989, Geo-Program—Program for geologic photogrammetry: The Compass, v. 66, no. 2, p. 59–64.

Daeholm, K.S., and Pillmore, C.L., 1989, Computer-assisted geologic photogrammetry: Photogrammetric Engineering and Remote Sensing, v. 55, p. 1191–1196.

Sawyer, D.A., Fleck, R.J., Lanphere, M.A., Warren, R.G., Broxton, D.E., and Hudson, M.R., 1994, Episodic caldera volcanism in the Miocene southwestern Nevada Volcanic Field—Revised stratigraphic framework, $^{40}Ar/^{39}Ar$ geochronology, and implications for magmatism and extension: Geological Society of America Bulletin, v. 106, p. 1304–1318.

Simonds, F.W., Whitney, J.W., Fox, K., Ramelli, A., Yount, J., Carr, M., Menges, C., Dickerson, R., and Scott, R.B., 1995, Map showing fault activity in the Yucca Mountain area, Nye County, Nevada: U.S. Geological Survey Miscellaneous Investigations Series Map I–2520, scale 1:24,000.

U.S. Department of Energy, 1988, Site characterization plan, Yucca Mountain Site, Nevada Research and Development, Nevada: Washington, D.C., U.S. Department of Energy Report DOE/RW–0199, 8 v. [variously paged].

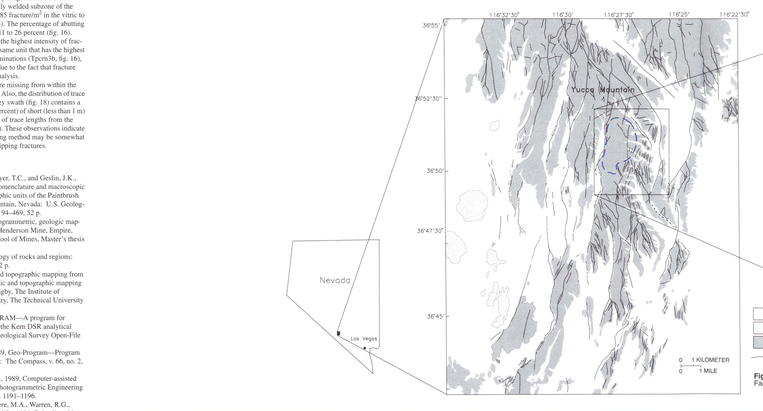

Figure 1. Map showing the location of Yucca Mountain, the Exploratory Studies Facility (ESF), and this mapping site. Faults are from Simonds and others (1995).

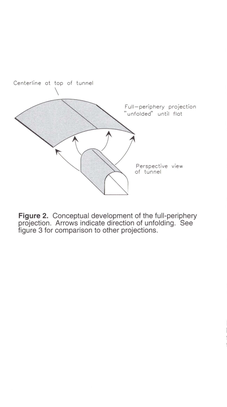

Figure 2. Conceptual development of the full-periphery projection. Arrows indicate direction of unfolding. See figure 3 for comparison to other projections.

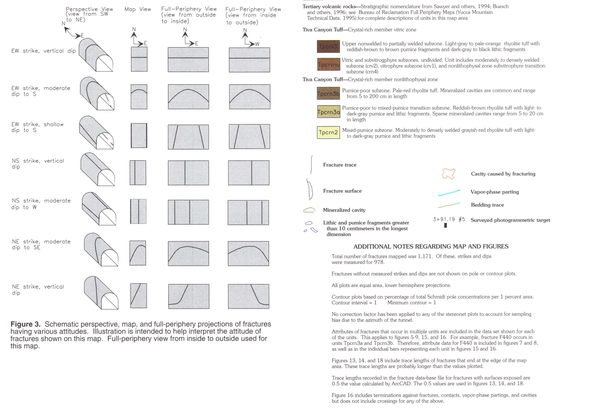

Figure 3. Schematic perspective, map, and full-periphery projections of fractures having various attitudes. Illustration is intended to help interpret the attitude of fractures shown on this map. Full-periphery view from inside to outside used for this map.

DESCRIPTION OF MAP UNITS

Tertiary(?) and Quaternary fracture filling

Fracture filling greater than 5 centimeters thick (white minerals unless noted otherwise)

Tertiary volcanic rocks—Stratigraphic nomenclature from Sawyer and others, 1994; Buesch and others, 1996; see Bureau of Reclamation Full Periphery Maps (Yucca Mountain Technical Data, 1995) for complete descriptions of units in this map area

Tiva Canyon Tuff—Crystal-rich member vitric zone

Tpcrvnu — Upper nonwelded to partially welded subzone. Light-gray to pale-orange rhyolite tuff with reddish-brown to brown pumice fragments and dark-gray to black lithic fragments

Tpcrn3b — Vitric and zeolitic/vapor-phase subzones, undivided. Unit includes moderately to densely welded subzone (crn3), vitric/vapor-phase subzone (crn3), and nonlithophysal zone subvitric/vapor transition subzone (crn4)

Tiva Canyon Tuff—Crystal-rich member nonlithophysal zone

Tpcrn3a — Pumice-poor subzone. Pale-red rhyolite tuff. Mineralized cavities are common and range from 5 to 200 cm in length

Tpcrn3c — Pumice-poor to mixed-pumice transition subzone. Reddish-brown rhyolite tuff with light- to dark-gray pumice and lithic fragments. Sparse mineralized cavities range from 5 to 20 cm in length

Tpcrn2 — Mixed-pumice subzone. Moderately to densely welded grayish-red rhyolite tuff with light- to dark-gray pumice and lithic fragments

ADDITIONAL NOTES REGARDING MAP AND FIGURES

Total number of fractures mapped was 1,171. Of these, strikes and dips were measured for 978.

Fractures without measured strikes and dips are not shown on pole or contour plots.

All plots are equal area, lower hemisphere projections.

Contour plots based on percentage of total Schmidt pole concentrations per 1 percent area. Contour interval = 3 Minimum contour = 1

No correction factor has been applied to any of the stereonet plots to account for sampling bias due to the azimuth of the tunnel.

Attributes of fractures that occur in multiple units are included in the data set shown for each of the units. The applies to figures 5-9, 15, and 16. For example, fracture F440 occurs in units Tpcrn3a and Tpcrn3b. Therefore, attribute data for F440 is included in figures 7 and 8, as well as in the individual lists representing each unit in figures 13 and 16.

Figures 13, 14, and 18 include trace lengths of fractures that end at the edge of the map area. These trace lengths are probably longer than the values plotted.

Trace lengths recorded in the fracture data-base file for fractures with surfaces exposed are 0.5 the value calculated by ArcCAD. The 0.5 values are used in figures 13, 14, and 18.

Figure 16 includes terminations against fractures, contacts, vapor-phase partings, and cavities but does not include crossings for any of the above.

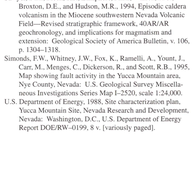
978 poles plotted
Maximum concentration = 5.83
POLE PLOT
DENSITY CONTOUR PLOT

Figure 4. Pole and density contour plots of attitudes of all fractures in all units.

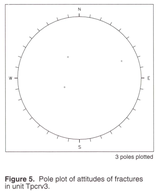
3 poles plotted
POLE PLOT
DENSITY CONTOUR PLOT

Figure 5. Pole plot of attitudes of fractures in unit Tpcrv3.

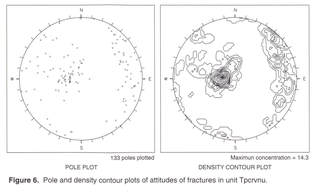
133 poles plotted
Maximum concentration = 14.3
POLE PLOT
DENSITY CONTOUR PLOT

Figure 6. Pole and density contour plots of attitudes of fractures in unit Tpcrvnu.

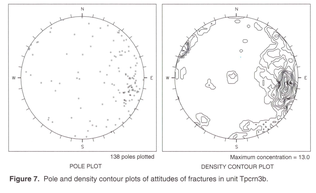
138 poles plotted
Maximum concentration = 13.0
POLE PLOT
DENSITY CONTOUR PLOT

Figure 7. Pole and density contour plots of attitudes of fractures in unit Tpcrn3b.

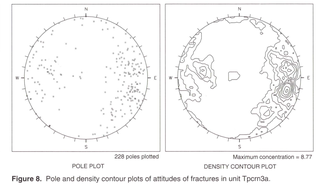
228 poles plotted
Maximum concentration = 8.77
POLE PLOT
DENSITY CONTOUR PLOT

Figure 8. Pole and density contour plots of attitudes of fractures in unit Tpcrn3a.

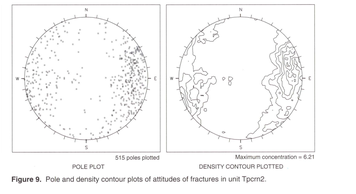
515 poles plotted
Maximum concentration = 6.21
POLE PLOT
DENSITY CONTOUR PLOTTED

Figure 9. Pole and density contour plots of attitudes of fractures in unit Tpcrn2.

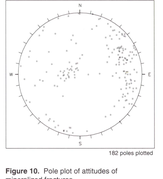
182 poles plotted

Figure 10. Pole plot of attitudes of mineralized fractures.

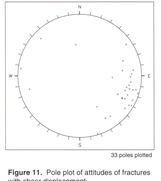
33 poles plotted

Figure 11. Pole plot of attitudes of fractures with shear displacement.

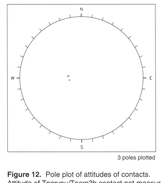
3 poles plotted

Figure 12. Pole plot of attitudes of contacts. Attitude of Tpcrvnu/Tpcrn3b contact not measured.

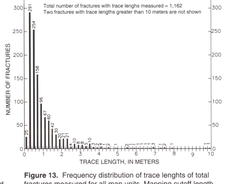

Figure 13. Frequency distribution of trace lengths of total fractures measured for all map units. Mapping cutoff length for measured fractures was approximately 15 centimeters.

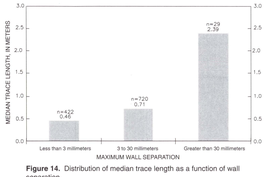

Figure 14. Distribution of median trace length as a function of wall separation.

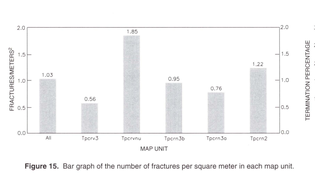

Figure 15. Bar graph of the number of fractures per square meter in each map unit.

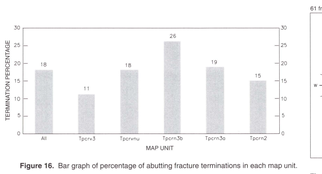

Figure 16. Bar graph of percentage of abutting fracture terminations in each map unit.

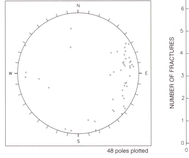
61 fractures mapped, 48 with measured strikes and dips
48 poles plotted

Figure 17. Pole plot of attitudes of fractures intersecting detailed line survey swath.

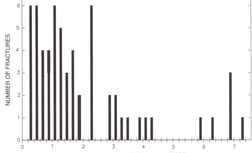

Figure 18. Frequency distribution of photogrammetrically measured trace lengths of fractures intersecting the detailed line survey swath.

GEOLOGIC MAP OF THE NORTH RAMP OF THE EXPLORATORY STUDIES FACILITY AT YUCCA MOUNTAIN, NEVADA, STATIONS 3+60 TO 4+25 METERS

by
JEFFREY A. COE

1997

[1]Use of trade names is for informational purposes only and does not constitute endorsement by the U.S. Geological Survey or the United States Government.

[2]When referred to in the "Results" section, all attitudes are given in degrees, using the right-hand rule convention.